INTERNATIONAL JOURNAL FOR NUMERICAL METHODS IN FLUIDS, VOL. 13, 507–518 (1991)

MULTIGRID FLOW SOLUTIONS IN COMPLEX TWO-DIMENSIONAL GEOMETRIES

D. RAYNER

Thermo-fluid Mechanics Research Centre, University of Sussex, Brighton BN1 9QT, U.K.

SUMMARY

A finite difference solution algorithm is described for use on two-dimensional curvilinear meshes generated by the solution of the transformed Laplace equation. The efficiency of the algorithm is improved through the use of a full approximation scheme (FAS) multigrid algorithm using an extended pressure correction scheme as smoother. The multigrid algorithm is implemented as a fixed V-cycle through the grid levels with a constant number of sweeps being performed at each grid level.

The accuracy and efficiency of the numerical code are validated using comparisons of the flow over two backward step configurations. Results show close agreement with previous numerical predictions and experimental data. Using a standard Cartesian co-ordinate flow solver, the multigrid efficiency obtainable in a rectangular system is shown to be reproducible in two-dimensional body-fitted curvilinear co-ordinates. Comparisons with a standard one-grid method show the multigrid method, on curvilinear meshes, to give reductions in CPU time of up to 93%.

KEY WORDS Multigrid Body-fitted co-ordinates

1. INTRODUCTION

In this paper a finite difference solution algorithm is described for use on two-dimensional curvilinear meshes. The meshes are generated by the solution of the transformed Laplace equation to produce a smooth variation between successive grid nodes. The method of solution outlined within this paper represents a stage in the development of the required solution algorithm. The motivation for the work is the gas turbine industry's interest in predictions of the fluid flow and heat transfer that take place in the compressor section of commercial gas turbine engines. Of particular interest is the heat transfer that takes place between the bottom of a stator blade and the rotating compressor drum.

Owing to irregular boundaries, there are a variety of flows of practical interest, such as in an axial compressor, for which rectangular meshes are unsuitable. Such domains require an alternative grid system that conforms to its boundaries. As these meshes are required to describe complex two-dimensional domains with refinement near the boundaries (to allow the accurate modelling of boundary layer flows, non-orthogonal body-fitted co-ordinates are used).

The CPU times necessary for convergence on such grids are generally expensive. In an effort to reduce the costs involved the multigrid acceleration technique of Brandt[1] has been applied to the solution method. For simplicity, the fluid under consideration has been taken as steady, laminar, incompressible and isothermal.

0271–2091/91/140507–12$06.00

Received May 1990
Revised October 1990

2. TRANSFORMATION OF THE GOVERNING EQUATIONS

For the given flow assumptions the momentum equations in the physical Cartesian co-ordinate plane are given by

$$\rho\frac{\partial}{\partial x}(u\phi)+\rho\frac{\partial}{\partial y}(v\phi)=-p_\phi+\mu\frac{\partial^2\phi}{\partial x^2}+\mu\frac{\partial^2\phi}{\partial y^2}, \tag{1}$$

where x, y denote the co-ordinate axes and ϕ $(=u, v)$ represents the relevant component of velocity; p_ϕ is the pressure gradient in the co-ordinate direction, μ is the viscosity and ρ is the density. Also, the continuity equation is given by

$$\frac{\partial u}{\partial x}+\frac{\partial v}{\partial y}=0. \tag{2}$$

Having obtained the physical (x, y)-mesh (Figure 1(a)) from the solution of the transformed Laplacian equation on the rectangular, non-uniform, body-fitted (ξ, η)-mesh (Figure 1(b)),[2] the equations of motion can be rewritten in the (ξ, η)-plane while maintaining the same dependent variables. Using the transformation described by Peyret and Viviand,[3] owing to the conservative form of the resulting equations, the momentum equations (1) are transformed to

$$\rho\frac{\partial}{\partial\xi}(U\phi)+\rho\frac{\partial}{\partial\eta}(V\phi)=-\hat{p}_\phi+\mu\frac{\partial}{\partial\xi}\left(\frac{q_1}{J}\frac{\partial\phi}{\partial\xi}+\frac{q_2}{J}\frac{\partial\phi}{\partial\eta}\right)+\mu\frac{\partial}{\partial\eta}\left(\frac{q_3}{J}\frac{\partial\phi}{\partial\eta}+\frac{q_2}{J}\frac{\partial\phi}{\partial\xi}\right), \tag{3}$$

where ξ, η are the transformed co-ordinate axes and U, V are the contravariant velocity components in the (ξ, η)-directions respectively. These relate to the covariant (u, v)-velocities by

$$U=uy_\eta-vx_\eta, \qquad V=vx_\xi-uy_\xi, \tag{4}$$

and the Jacobian, J of the transformation between the physical co-ordinate system and the transformed co-ordinate system is defined as

$$J=x_\xi y_\eta-x_\eta y_\xi, \tag{5}$$

the subscript denoting the partial derivative of first order. Also in equation (3) the geometric relations (q_1, q_2, q_3) and the transformed pressure gradient terms $(\hat{p}_\phi)$ are given by

$$\begin{gathered} q_1=x_\eta^2+y_\eta^2, \qquad q_2=-x_\xi x_\eta-y_\xi y_\eta, \qquad q_3=x_\xi^2+y_\xi^2, \\ \hat{p}_u=y_\eta p_\xi-y_\xi p_\eta, \qquad \hat{p}_v=x_\xi p_\eta-x_\eta p_\xi. \end{gathered} \tag{6}$$

Similarly, the transformation of the continuity equation (2) is given by

$$\frac{\partial U}{\partial\xi}+\frac{\partial V}{\partial\eta}=0. \tag{7}$$

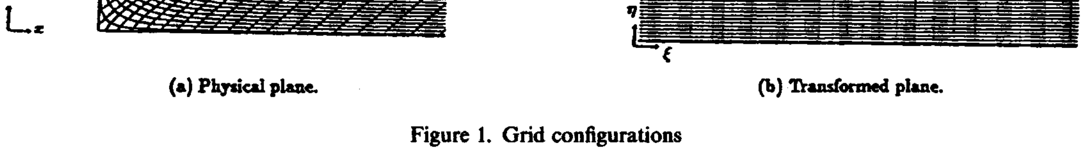

(a) Physical plane. (b) Transformed plane.

Figure 1. Grid configurations

3. NUMERICAL SOLUTION METHOD

In the discretization of the momentum and continuity equations the staggered mesh of Harlow and Welch[4] is used. This involves staggering the location of the velocity components half a step size back (in the appropriate co-ordinate direction) from the location of the pressure nodes (Figure 2) to prevent a 'chequerboard' pressure field resulting.[5]

3.1. Velocity and pressure corrections

Following the SIMPLEC formulation of Van Doormaal and Raithby,[6] corrections to the guessed velocity fields are made based upon corrections to the guessed pressure field. Braaten and Shyy[7] found that correcting the contravariant velocity components and using these to make corrections to u, v, rather than vice versa, led to greater stability of the solution algorithm and allowed lower attainable values of the mass residual. Thus the corrections to the guessed contravariant velocity fields are obtained (using the notation relative to the appropriate velocity location) from

$$U=U^*+\frac{p'_{\mathrm{w}}-p'_{\mathrm{e}}}{\Delta\xi}(d_u y_\eta^2+d_v x_\eta^2)+\frac{p'_{\mathrm{n}}-p'_{\mathrm{s}}}{\Delta\eta}(d_u y_\xi y_\eta+d_v x_\xi x_\eta), \tag{8}$$

$$V=V^*+\frac{p'_{\mathrm{s}}-p'_{\mathrm{n}}}{\Delta\eta}(d_u y_\xi^2+d_v x_\xi^2)+\frac{p'_{\mathrm{e}}-p'_{\mathrm{w}}}{\Delta\xi}(d_u y_\xi y_\eta+d_v x_\xi x_\eta), \tag{9}$$

where ϕ^* denotes the guessed value of ϕ, ϕ' denotes the correction made to ϕ and

$$d_u=\frac{1}{a_{\mathrm{p}}-\alpha_u\sum a_{\mathrm{nb}}}, \qquad d_v=\frac{1}{a_{\mathrm{p}}-\alpha_v\sum a_{\mathrm{nb}}}. \tag{10}$$

In their present form equations (8) and (9) would give a pressure correction equation whose source term contains reference to a number of pressure nodes not contained within the usual five-

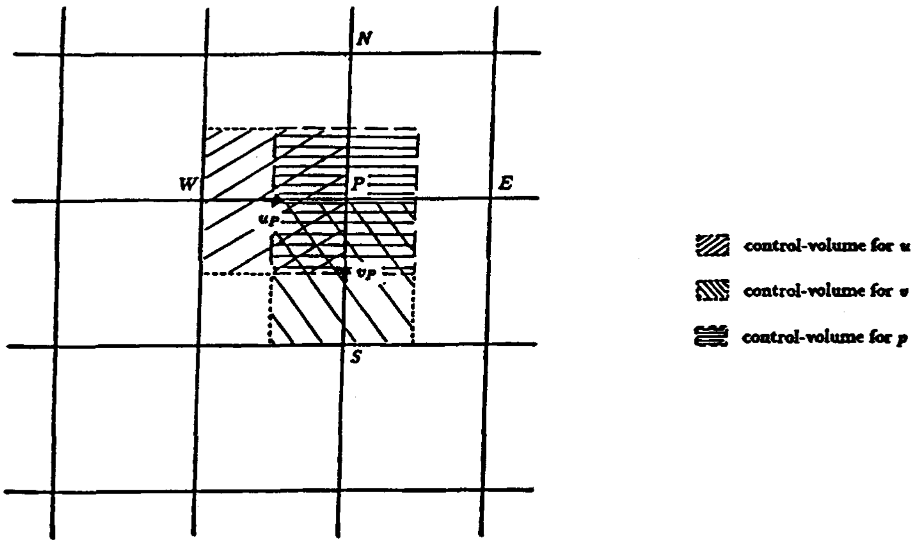

Figure 2. Location of the staggered variables

point scheme. Thus an accurate representation of the source term would require repeated solution of the pressure correction equation for the five-point scheme to be retained. Shyy *et al.*,[8] however, found that neglecting the cross-multiplied geometric terms ($x_\xi x_\eta$ and $y_\xi y_\eta$) in equations (8) and (9) gave faster convergence rates and reduced the source term to the mass imbalance through the control volume. The omission of such terms does not constitute a loss of accuracy, since such terms are relatively small and because the source term of the pressure correction equation tends to zero as the velocity fields converge. Hence corrections to U, V are obtained from

$$U = U^* + \frac{p'_w - p'_e}{\Delta\xi}(d_u y_\eta^2 + d_v x_\eta^2), \tag{11}$$

$$V = V^* + \frac{p'_s - p'_n}{\Delta\eta}(d_u y_\xi^2 + d_v x_\xi^2). \tag{12}$$

Analytically, the corrections to u, v can be found from the inversion of equations (4) as

$$u = \frac{1}{J}(U x_\xi + V x_\eta), \tag{13}$$

$$v = \frac{1}{J}(U y_\xi + V y_\eta). \tag{14}$$

However, owing to the interpolation required for the staggering of the velocity components, equations (13) and (14) would introduce an inconsistency between the (U, V)- and (u, v)-velocity fields. In matrix notation equations (4) could be written as

$$\mathbf{Mu} = \mathbf{U}, \tag{15}$$

and so a consistent way of correcting the (u^*, v^*)-velocities could be obtained from the corrected contravariant velocities via equation (15) as

$$\mathbf{u} = \mathbf{M}^{-1}\mathbf{U}. \tag{16}$$

Since $\mathbf{M}$ is a large, sparse matrix and the (u^*, v^*)-velocities need to be corrected from U, V at the end of each iteration, the use of matrix inversion or direct solution procedures is impractical. Also, $\mathbf{M}$ is not guaranteed to be diagonally dominant and so iterative methods would be costly. Thus the (u^*, v^*)-velocity fields are corrected via a number of D'yakanov iterations[7] as follows.

The problem is first reformulated in the form

$$\mathbf{H}(\mathbf{u} - \mathbf{u}^*) = \mathbf{U} - \mathbf{Mu}^*, \tag{17}$$

where $\mathbf{u}^*$ represents the guessed value of $\mathbf{u}$. If the matrix $\mathbf{H}$ is similar to the matrix $\mathbf{M}$, then an iterative method of this type can be shown to converge very quickly. A suitable matrix $\mathbf{H}$ can be found from the calculation of the inconsistent (u, v)-velocities using equations (13) and (14). In matrix notation these equations can be expressed as

$$\tilde{\mathbf{u}} = \mathbf{GU}, \tag{18}$$

where the tilde is used to indicate that $\tilde{\mathbf{u}}$ is not consistent with equation (15) because of interpolation errors. In the limit the interpolation errors would vanish as the mesh size is reduced to zero, so $\tilde{\mathbf{u}} \rightarrow \mathbf{u}$. Hence in the limit of zero mesh size we would have

$$\mathbf{G}^{-1}\tilde{\mathbf{u}} \rightarrow \mathbf{G}^{-1}\mathbf{u} = \mathbf{U} = \mathbf{Mu}, \tag{19}$$

so that

$$\mathbf{G}^{-1}\rightarrow\mathbf{M}. \tag{20}$$

For a finite mesh size $\mathbf{G}^{-1}$ serves as a close approximation to $\mathbf{M}$ and hence is a suitable choice for $\mathbf{H}$. Equation (17) thus becomes

$$\mathbf{G}^{-1}(\mathbf{u}-\mathbf{u}^*)=\mathbf{U}-\mathbf{M}\mathbf{u}^*, \tag{21}$$

which, premultiplied by $\mathbf{G}$, gives

$$\mathbf{u}=\mathbf{u}^*+\mathbf{G}\mathbf{U}-\mathbf{G}(\mathbf{M}\mathbf{u}^*). \tag{22}$$

By treating the current value of u, v as the new guessed values, the repeated solution of equation (22) provides a consistent means by which the guessed (u, v)-velocities can be corrected from the updated contravariant velocities. In practice the use of this method is found to converge very quickly and adds little to the overall CPU time of the solution algorithm.

3.2. The multigrid algorithm

The multigrid method of Brandt[1] has been found to be very efficient in the solution of fluid dynamics problems. The particular method used, a FAS multigrid algorithm implemented as a fixed V-cycle, is outlined below.

The non-linear, partial differential equations of motion $(N(\phi)=f)$ are represented in discrete form on a fine mesh M_k by

$$N_k(\phi_k)=f_k. \tag{23}$$

Unless the dependent variables are correct, there is a defect associated with each variable at each mesh point within the solution domain, given by

$$d_k=f_k-N_k(\phi'_k), \tag{24}$$

where ϕ'_k is the current approximation to ϕ_k. If we assume a correction ψ_k which needs to be added to ϕ'_k to complete the solution, the original equations (23) can be rewritten as defect equations

$$N_k(\phi'_k+\psi_k)=d_k+N_k(\phi'_k). \tag{25}$$

The fine grid solution is then smoothed using the pressure correction method. This gives negligible high-frequency errors compared to the low-frequency errors. The defect equations (25) are then represented on a coarser mesh M_{k+1} by

$$N_{k+1}(\phi'^{o}_{k+1}+\psi_{k+1})=d^{o}_{k+1}+N^{o}_{k+1}(\phi'^{o}_{k+1}), \tag{26}$$

where x^{o}_{k+1} denotes the restricted value of x_k. If we note that equation (26) is of the form of equation (23), the process can be repeated to a coarser mesh M_{k+2} and so on. On the coarsest mesh M_{k+h} an equation of the form (26) can then be solved to give corrections needed to the coarsest mesh solution, ψ_{k+h}. These corrections are then interpolated back onto successively finer meshes by the repeated solution of

$$\psi'_i=I(\psi_{i+1}), \tag{27}$$

where I is an interpolation operator, to eventually give an approximation to the fine mesh corrections ψ_k. At each interpolation the equations are again smoothed using the pressure correction method. A new approximation to the fine grid solution ϕ_k can then be found from

$$\phi''_k=\phi'_k+\psi'_k. \tag{28}$$

Unlike a one-grid method, the multigrid method is expected to give grid-independent convergence, so that the number of iterations required to achieve a converged solution is independent of the fine mesh size. Thus, as the number of mesh nodes increases, the multigrid method is expected to give increasing savings in CPU time over the one-grid method.

3.3. *The solution procedure*

A finite difference representation of the equations of motion is made on a staggered, non-uniform, rectangular (ξ, η)-mesh employing the 'hybrid' upwinding scheme of Patankar and Spalding.[9] The momentum equations are then solved using one sweep of an alternating direction, five-point TDMA solver. Implicit underrelaxation is used in the solution of the momentum equations, via the coefficients, owing to their non-linearity. Explicit underrelaxation is used for the pressure correction, but no relaxation is required for the calculation of the contravariant velocities. The derivative terms such as x_ξ are calculated by second-order differencing at each location they are required. The geometric terms, q_1, q_2, q_3, on the other hand, are only calculated at the major grid nodes and interpolated, where required, to the control volume faces. This is consistent with the technique used by Shyy *et al.*,[8] who found this to be a more accurate way of fulfilling the physical conservation laws. Following the update of the contravariant velocities, a number of sweeps of the pressure correction equation are performed to smooth the solution. The velocities are then updated via the velocity correction equations and a number of D'yakanov iterations, and the guessed pressure field is updated. This defines one relax sweep.

After a number of relax sweeps the defects are computed from equation (25). The variables and their defects are then restricted down onto the next coarsest mesh. The coarse grids and the coarse mesh location of the physical co-ordinates (x, y) are generated by simply omitting every other principal node in each direction, the velocities being staggered as on the fine mesh. The derivative terms and geometric terms are then calculated as before on the coarse mesh and the contravariant velocities recalculated. A nine-point grid-weighted restriction operator is used for the variables and defects at the principal nodes. For the staggered velocities a six-point operator is employed, since their coarse grid positions are not coincident with any of the fine grid except at the boundaries.

Equations (26) are then smoothed and the procedure repeated until the coarsest mesh is reached, on which a large number of relax sweeps are used in order to obtain a reasonable solution. After the corrections have been calculated they are prolonged to the next finest mesh by bilinear interpolation. The contravariant velocities are then calculated from the interpolated (u, v)-velocities and the equations smoothed using a number of sweeps before interpolation to the next finest level. An extra stability measure is introduced by underrelaxing the corrections, so that equation (28) is replaced by

$$\phi''_k = \phi'_k + \beta \psi'_k, \tag{29}$$

which allows fewer relax sweeps (since it allows a less smooth solution) than would otherwise be necessary to achieve convergence. By repeating the process, the corrections to the fine mesh solution are eventually obtained.

3.4. *Boundary conditions*

The test cases considered within this paper have dimensions chosen to facilitate comparison with other authors and so that known velocity fields can be prescribed at the boundaries. The boundary conditions at solid walls are set using the no-slip condition. A uniform velocity $(\bar{u})$ is set at inlet and a fully developed velocity profile at outlet. At both these boundaries the v-velocity component is set via the continuity equation (2). Pressure boundaries are set so that no pressure correction takes place at any of the boundaries.

4. RESULTS

In the solution of the test cases considered, underrelaxation factors of 0·6 are used for the momentum equations (α_u, α_v), 1·0 for the pressure correction equation (α_p) and 0·8 for the multigrid corrections (β). Also, two relax sweeps are performed in moving between the grid levels, and six relax sweeps performed on the coarsest mesh. For the curvilinear mesh solutions only one D'yakanov iteration is applied, and for both mesh configurations five pressure sweeps are used for the augmented backward step test case and two for the backward step test case.

4.1. Flow over an augmented backward step

A schematic representation of the physical domain for this test case is shown in Figure 3(a). Using comparisons with previous authors' findings, the augmented backward step test case has been chosen to validate the accuracy of the transformed computer code. Reynolds numbers ($Re_h = h\bar{u}/\nu$, where h is the step height and ν is the kinematic viscosity) of 73 and 229 are chosen.

Solutions are obtained on curvilinear meshes with 129 × 65, 65 × 33 and 33 × 17 interior grid nodes. The distributions of the grid nodes within the solution domain are chosen so as to give refinement in the region of the step. All test cases are started from the initial conditions of zero flow. Convergence is taken when the largest root-mean-square (RMS) change of the normalized variables falls below a tolerance level of $2{\cdot}5 \times 10^{-5}$.

Figure 4 shows a velocity profile comparison with the numerical predictions of Atkins *et al.*[10] and the experimental results of Denham and Patrick.[11] The current numerical predictions on a 129 × 65 mesh show a close agreement with the findings of the above authors. Figure 5 shows a comparison of the length of the recirculation zone with the Reynolds number. The reattachment length (L_R) is measured from the step face to the point of reattachment. Additional computations at Reynolds numbers of 10, 50, 100, 125, 150, 175 and 200 have been performed using 129 × 65 grid nodes to give a more complete comparison. Again the current numerical predictions show good agreement with the findings of Atkins *et al.* and Denham and Patrick.

A summary of the performance of this test cases is given in Tables I and II for Reynolds numbers of 73 and 229 respectively. The CPU times quoted are for the VAX 8530 computer. The solutions give grid-independent convergence with significant reductions in CPU time over the one-grid method. The reductions in CPU time are seen to increase with increased grid size, with

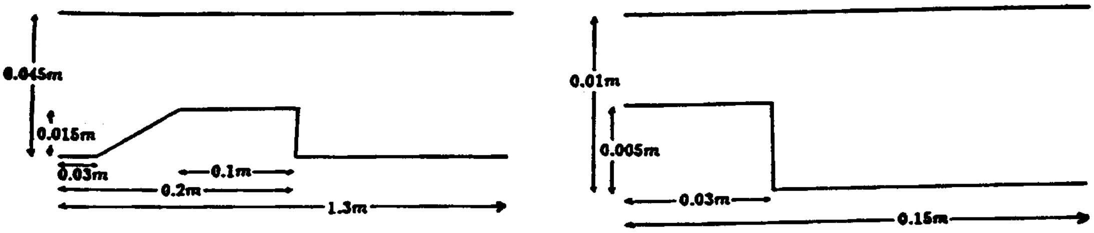

(a) Augmented backward step.

(b) Backward step.

Figure 3. Test case configurations

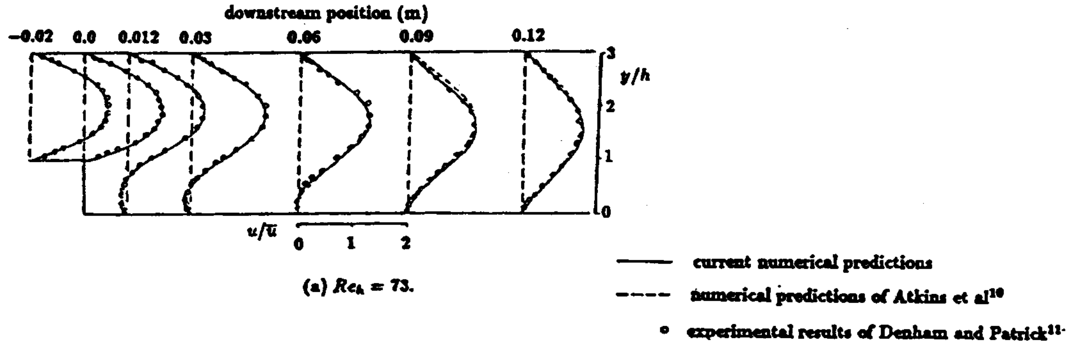

(a) $Re_h = 73$.

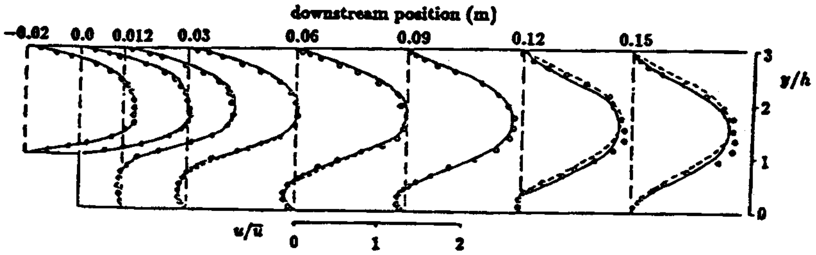

(b) $Re_h = 229$.

Figure 4. Velocity profile comparison

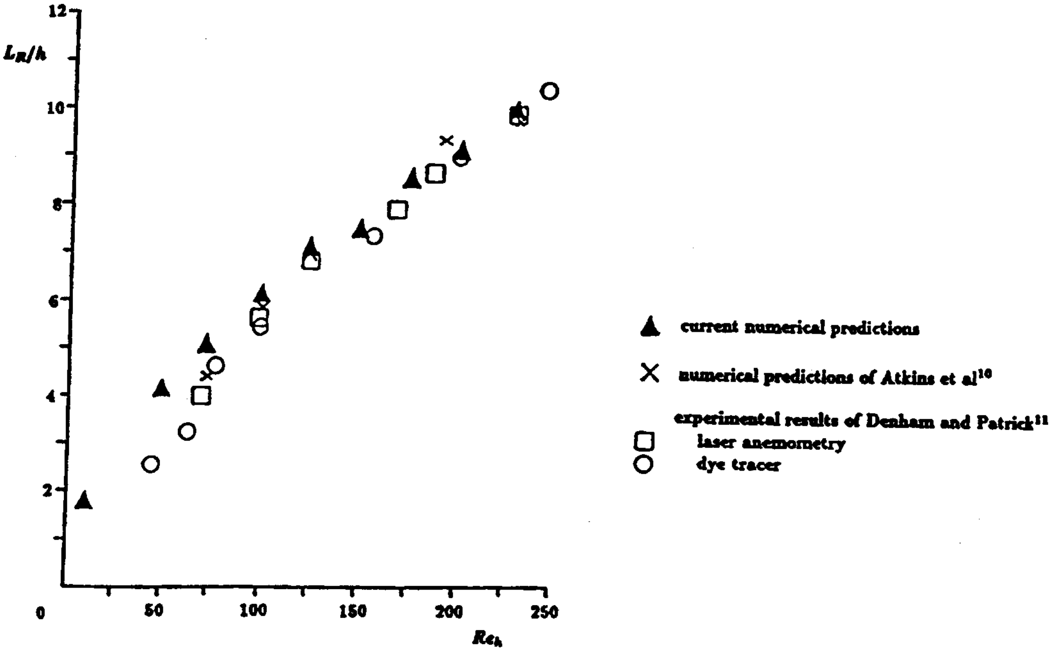

Figure 5. Reattachment length comparison

Table I

Grid size	No. of grid levels	Iterations required	CPU time required
33 × 17	1	113	00:01:55
	2	12	00:01:19
65 × 33	1	314	00:19:16
	3	14	00:05:46
129 × 65	1	671	02:53:22
	4	14	00:23:14

Table II

Grid size	No. of grid levels	Iterations required	CPU time required
33 × 17	1	129	00:02:13
	2	18	00:01:56
65 × 33	1	262	00:16:17
	3	17	00:07:00
129 × 65	1	616	02:39:41
	4	19	00:32:00

an average saving of 22% on a 33 × 17 mesh, a 64% saving on a 65 × 33 mesh and up to an 87% saving on a 129 × 65 mesh.

4.2. Flow over a backward step

A schematic representation of the physical domain for this test case is shown in Figure 3(b). This test case has been chosen to compare the body-fitted co-ordinate solutions with the standard rectangular co-ordinate solutions. Reynolds numbers of 50 and 150 are chosen. Solutions are obtained on curvilinear and rectangular meshes with 129 × 65, 65 × 33 and 33 × 17 interior grid nodes. The arrangements of the rectangular grids are chosen so as to be comparable with the curvilinear grids.

The convergence of the multigrid and one-grid methods for both grid configurations is shown in Figures 6(a) and 6(b), $\overline{Res}$ being used to denote the average RMS of the normalized residuals. These show that both mesh arrangements gave similar convergence characteristics and graphically demonstrate the benefits of the monotonic convergence of the multigrid method over the one-grid method. Figure 7 shows a comparison of the predicted shear stress on both 129 × 65 mesh configurations. The wall co-ordinate is taken as the distance along the lower boundary. There is seen to be a very close agreement between the curvilinear and rectangular mesh solutions.

Tables III and IV give a summary of the test case performance for Reynolds numbers of 50 and 150 respectively. In the multigrid method the number of grid levels used is the same as in the previous test case. Both the curvilinear and rectangular mesh solutions show the multigrid method to give nearly grid-independent convergence and to be beneficial over the one-grid method. The curvilinear mesh gave an average multigrid saving of 44% compared to 62% on a rectangular mesh using 33 × 17 grid nodes, 74% compared to 83% using 65 × 33 grid nodes and 93% compared to 94% using 129 × 65 grid nodes. Thus similar savings in CPU time are obtained

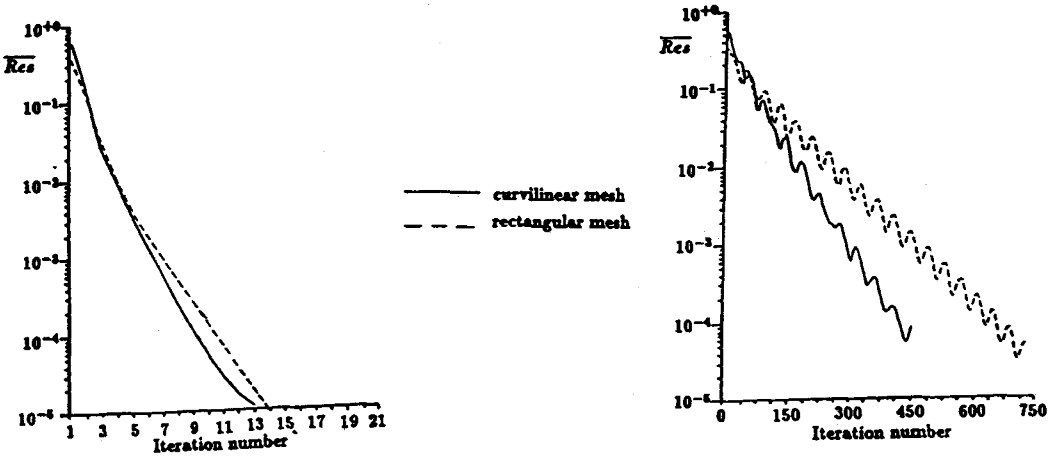

(a) multigrid (b) one-grid

Figure 6. Convergence characteristics for $Re_h = 50$

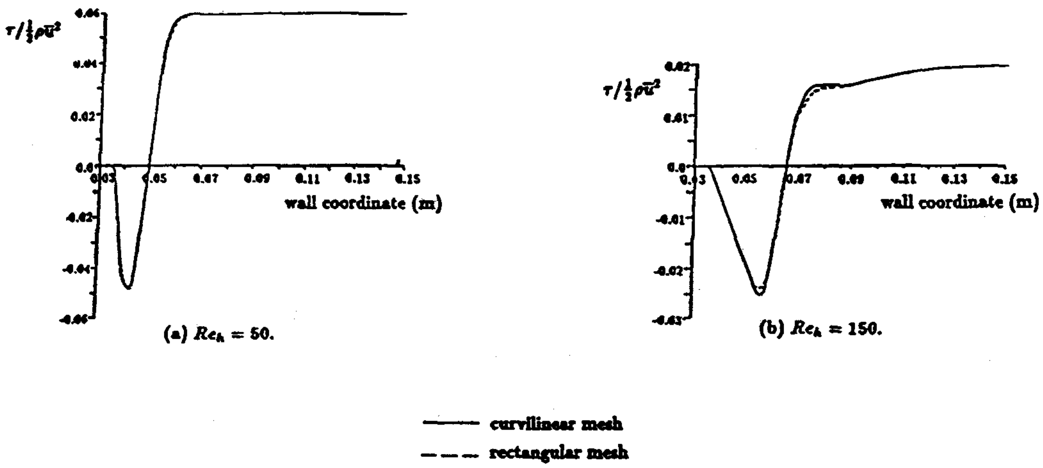

(a) $Re_h = 50.$ (b) $Re_h = 150.$

Figure 7. Shear stress comparison

Table III

Grid size	Grid configuration	Iterations required		CPU time required	
		One-grid	Multigrid	One-grid	Multigrid
33 × 17	Curvilinear	176	11	00:02:33	00:01:02
	Rectangular	273	12	00:02:57	00:00:56
65 × 33	Curvilinear	455	13	00:24:26	00:04:35
	Rectangular	725	14	00:28:56	00:04:00
129 × 65	Curvilinear	2247	20	08:26:33	00:28:22
	Rectangular	2722	20	07:19:25	00:22:07

Table IV

Grid size	Grid configuration	Iterations required		CPU time required	
		One-grid	Multigrid	One-grid	Multigrid
33 × 17	Curvilinear	152	17	00:02:10	00:01:33
	Rectangular	238	15	00:02:35	00:01:08
65 × 33	Curvilinear	353	18	00:18:58	00:06:21
	Rectangular	615	18	00:24:49	00:05:01
129 × 65	Curvilinear	1484	20	05:34:32	00:28:16
	Rectangular	2007	23	05:22:22	00:24:55

from the use of the multigrid method on both mesh configurations, although direct comparisons are difficult since the rectangular mesh solutions contain fewer grid nodes within the solution domain owing to the blocking required.

5. CONCLUSIONS

A multigrid method using an extended pressure correction scheme as smoother is presented for flows on non-orthogonal grids generated by the inversion of Laplace's equation. The efficiency and accuracy of the transformed computer code are verified using comparisons for the flow over two backward step configurations. Comparisons with a one-grid method show the multigrid method to be substantially more efficient, and using a standard rectangular flow solver, the multigrid efficiency obtainable in rectangular systems is shown to be reproducible in body-fitted co-ordinates.

The results obtained represent a stage in the development of the required solution algorithm. Thus the convergence and accuracy of the current numerical code do not necessarily represent the optimum values and with further investigation may be improved upon. The results obtained, however, provide an encouraging base from which to extend the method to more realistic flow properties in complex three-dimensional cylindrical polar geometries.

ACKNOWLEDGEMENTS

The author would like to acknowledge the assistance of Drs. C. M. Vaughan and S. Gilham and the financial support of Ruston Gas Turbines Ltd.

REFERENCES

1. A. Brandt, 'Multigrid techniques: 1984 guide with applications to fluid dynamics', *GMD-Studien, Nr. 85*, Bonn, 1984.
2. D. Rayner, 'Multigrid solutions of laminar flows in body-fitted curvilinear coordinates', *University of Sussex Report 89/TFMRC/121*, 1989.
3. R. Peyret and H. Viviand, 'Computation of viscous compressible flows based on the Navier–Stokes equations', *AGARD-AG-212*, 1975.
4. F. H. Harlow and J. E. Welch, 'Numerical calculation of time dependent viscous incompressible flow of fluid with free surface', *Phys. Fluids*, **8**, 2182–2189 (1965).
5. S. V. Patankar, *Numerical Heat Transfer and Fluid Flow*, McGraw-Hill, New York, 1980.
6. J. P. Van Doormaal and G. D. Raithby, 'Enhancements of the SIMPLE method for predicting incompressible fluid flows', *Numer. Heat Transfer*, **7**, 147–163 (1984).
7. J. M. Braaten and W. Shyy, 'A study of recirculating flow computation using body-fitted coordinates: consistency aspects and mesh skewness', *Numer. Heat Transfer*, **9**, 559–574 (1986).

8. W. Shyy, S. S. Tong and S. M. Correa, 'Numerical recirculation flow calculation using a body-fitted coordinate system', *Numer. Heat Transfer*, **8**, 99–113 (1985).
9. S. V. Patankar and D. B. Spalding, 'A calculation procedure for heat and mass transfer in three-dimensional parabolic flows', *Int. J. Heat Mass Transfer*, **15**, 1787–1806 (1972).
10. D. J. Atkins, S. J. Maskell and M. A. Patrick, 'Numerical prediction of separated flows', *Int. j. numer. methods eng.*, **15**, 129–144 (1980).
11. M. K. Denham and M. A. Patrick, 'Laminar flow over a downstream-facing step in a two-dimensional flow channel', *Trans. Inst. Chem. Eng.*, **52**, 361–367 (1974).